European Journal of Pharmaceutics and Biopharmaceutics 80 (2012) 682–689

Contents lists available at SciVerse ScienceDirect

European Journal of Pharmaceutics and Biopharmaceutics

journal homepage: www.elsevier.com/locate/ejpb

Research paper

Mechanistic modelling of the drying behaviour of single pharmaceutical granules

Séverine Thérèse F.C. Mortier [a,b,*], Thomas De Beer [b], Krist V. Gernaey [c], Jurgen Vercruysse [d], Margot Fonteyne [b], Jean Paul Remon [d], Chris Vervaet [d], Ingmar Nopens [a]

[a] BIOMATH, Department of Mathematical Modelling, Statistics and Bioinformatics, Ghent University, Ghent, Belgium
[b] Department of Pharmaceutical Analysis, Ghent University, Ghent, Belgium
[c] Department of Chemical and Biochemical Engineering, Technical University of Denmark, Lyngby, Denmark
[d] Department of Pharmaceutics, Ghent University, Ghent, Belgium

ARTICLE INFO

Article history:
Received 14 September 2011
Accepted in revised form 20 December 2011
Available online 31 December 2011

Keywords:
Mechanistic modelling
Drying
Porous material
Pharmaceutical granules
Model calibration
Model validation

ABSTRACT

The trend to move towards continuous production processes in pharmaceutical applications enhances the necessity to develop mechanistic models to understand and control these processes. This work focuses on the drying behaviour of a single wet granule before tabletting, using a six-segmented fluidised bed drying system, which is part of a fully continuous from-powder-to-tablet manufacturing line. The drying model is based on a model described by Mezhericher et al. [1] and consists of two submodels. In the first drying phase (submodel 1), the surface water evaporates, while in the second drying phase (submodel 2), the water inside the granule evaporates. The second submodel contains an empirical power coefficient, β. A sensitivity analysis was performed to study the influence of parameters on the moisture content of single pharmaceutical granules, which clearly points towards the importance of β on the drying behaviour. Experimental data with the six-segmented fluidised bed dryer were collected to calibrate β. An exponential dependence on the drying air temperature was found. Independent experiments were done for the validation of the drying model.

1. Introduction

1.1. Towards continuous pharmaceutical processing

Traditionally, the pharmaceutical industry has mainly relied on batch processing [2]. However, currently the intention and opportunity exist to take the step to move towards continuous production processes [2]. Assuming that the same amount of product needs to be produced, the equipment in a continuous production process will typically be significantly smaller compared to a batch process. In addition, continuous production processes are based on the one-in–one-out principle, avoid scale-up issues, reduce cycle times, reduce production costs, ensure faster product release, reduce variability, increase flexibility and efficiency, and improve product quality [2–4]. However, continuous manufacturing does not always have advantages over batch processes [4,5]. As a consequence of slow reaction kinetics, to name one important example, Roberge et al. expected that only 50% of the reactions carried out at Lonza would benefit from continuous operation [6].

It is obvious that the conventional quality control systems of production processes based on off-line analyses in analytical laboratories would to a large extent eliminate the advantages of continuous processing and that continuous real-time quality control is indispensable for continuous production. For the implementation of advanced process control systems relying on in-process measurements of critical process and product parameters and real-time adjustment of input variables, it is necessary to understand each unit operation in detail. A mechanistic model is useful in this respect to understand the influence of input variables and detect the most critical variables [2–4]. The importance of using mechanistic models and systems-based approaches in a Process Analytical Technology (PAT) and a Quality By Design (QbD) context therefore been acknowledged [7–9].

The production of tablets consists of several consecutive steps and starts with the blending of the individual components, that is, the Active Pharmaceutical Ingredient (API) s and the excipients. Granulation, to agglomerate the particles into granules, is the next step. The purpose is to improve the flowability, processability, etc. of the raw materials. Several granulation techniques exist: wet granulation, dry granulation, melt granulation, etc. [10]. Incorporating a

* Corresponding author. BIOMATH, Department of Mathematical Modelling, Statistics and Bioinformatics, Faculty of Bioscience Engineering, Ghent University, Coupure Links 653, 9000 Ghent, Belgium. Tel.: +32 (0)9 264 61 96; fax: +32 (0)9 264 62 20.

E-mail addresses: severine.mortier@ugent.be (S.T.F.C. Mortier), thomas.debeer@ugent.be (T. De Beer), KVG@kt.dtu.dk (K.V. Gernaey), jurgen.vercruysse@ugent.be (J. Vercruysse), margot.fonteyne@ugent.be (M. Fonteyne), jeanpaul.remon@ugent.be (J.P. Remon), chris.vervaet@ugent.be (C. Vervaet), ingmar.nopens@ugent.be (I. Nopens).

URL: http://biomath.ugent.be (S.T.F.C. Mortier).

0939-6411/$ - see front matter © 2011 Elsevier B.V. All rights reserved.
doi:10.1016/j.ejpb.2011.12.010

wet granulation operation in the tabletting production process requires the drying of the wet granules afterwards. A drying step is performed to remove the granulation solvent. As a consequence, another import aspect is the influence of the drying step on granule specs. The choice of the technique for drying wet granules might influence the properties of the granules and, hence, the further downstream processing [11]. After drying the dry granules can eventually undergo a milling step and/or a post-blending step, after which the tabletting step is performed [4].

1.2. Drying model

Several methods have been reported in literature to model the drying behaviour of granules. An extensive review can be found in [4]. This work focuses on the drying behaviour of a single wet granule using a six-segmented fluidised bed drying system, which is part of a fully continuous from-powder-to-tablet manufacturing line (ConsiGma™, Collette™, GEA Pharma Systems). Taking into account the size of pharmaceutical granules (0.1–2 mm), produced continuously using the continuous twin-screw granulator, models for drying processes of single particles were chosen for the work described here. The continuum approach [12–15] and the pore network models [16–19] describe how water is evolving in the porous material, while such detailed information is really not necessary for the drying of the particles studied here. In this project, there is an interest in describing the dynamics of the moisture content of a certain mass (20–100 g) of continuously produced granules (i.e., a segment of the six-segmented fluidised bed dryer filled with granules).

A mechanistic model for the description of drying processes of single granules was found in the literature [1,20]. This model describes the drying of a motionless single porous droplet in a flow of atmospheric air and consists of two drying phases. A droplet consists of a wet porous particle surrounded by a water layer at the surface. The model takes the time-dependent character of the heat transfer during the drying process into account. The temperature profile within the wet particle is calculated during drying. The crust region, formed in the second drying period (i.e., when the surrounding water is removed), is responsible for the resistance to diffusion mass transfer, dependent on the crust porosity, and heat absorption. The temperature dependence of physical properties (such as the specific heat, the coefficient of vapour diffusion, and the specific heat of evaporation) is taken into account during drying, using the temperature of the granule. In the first drying phase, the water from the droplet surface evaporates. The second drying phase begins when the radius of the droplet equals the radius of the dry particle. In the second phase, two regions are formed: a wet core and a dry crust. The vapour, evaporated at the interface between the wet core and the dry crust, diffuses through the crust pores until it exits the pores and forms a thin boundary layer over the particle surface. This vapour is removed through advection by the air flow.

In the first drying period, a uniform droplet temperature profile is assumed. The evaporation rate in the first drying phase is calculated by:

$$\dot{m}_v = h_D(\rho_{v,s} - \rho_{v,\infty})A_d \tag{1}$$

where $\dot{m}_v$ is the mass transfer rate, h_D the mass transfer coefficient, $\rho_{v,s}$ the partial vapour density over the droplet surface, $\rho_{v,\infty}$ the partial vapour density in the ambient air, and A_d the surface area of the droplet [20].

In the second drying phase, the evaporation rate is given by:

$$\dot{m}_v = -\frac{8\pi\epsilon^{\beta}D_{v,cr}M_w p_g}{\Re(T_{cr,s}+T_{wc,s})} ln\left[\frac{p_g - p_{v,i}}{p_g - \left(\frac{\Re}{4\pi M_w h_D R_p^2}\dot{m}_v + \frac{p_{v,\infty}}{T_g}\right)T_{p,s}}\right] \tag{2}$$

with ϵ the crust porosity, β an empirical power coefficient, $D_{v,cr}$ the vapour diffusion coefficient (crust pores), M_w the molecular weight of the liquid, p_g the pressure of the drying agent, $T_{cr,s}$ and $T_{wc,s}$, respectively, the temperature of the crust outer surface and of the crust-wet core interface, $p_{v,i}$ and $p_{v,\infty}$, respectively, the partial vapour pressure at the crust-wet core interface and in the ambient air, h_D the mass transfer coefficient, R_p the particle radius, and T_g the temperature of the drying agent.

These equations have to be solved simultaneously with an Ordinary Differential Equation (ODE) for the decrease in droplet radius, an ODE for the temperature of the droplet, an ODE for the decrease in wet core radius, a Partial Differential Equation (PDE) for the temperature profile in the dry crust, and a PDE for the temperature profile in the wet core [1]. The equations are reproduced for the reader's convenience (Eqs. (3)–(7)).

$$\frac{dR_d}{dt} = -\frac{1}{\rho_w 4\pi R_d^2}\dot{m}_v \tag{3}$$

$$h_{fg}\dot{m}_v + c_{p,w}m_d\frac{dT_d}{dt} = h(T_g - T_d)4\pi R_d^2 \tag{4}$$

$$\frac{dR_i}{dt} = -\frac{1}{\epsilon\rho_w 4\pi R_i^2}\dot{m}_v \tag{5}$$

$$\rho_{wc}c_{p,wc}\frac{\partial T_{wc}}{\partial t} = \frac{1}{r^2}\frac{\partial}{\partial r}\left(k_{wc}r^2\frac{\partial T_{wc}}{\partial r}\right), \quad 0 \leqslant r \leqslant R_i(t) \tag{6}$$

$$\frac{\partial T_{cr}}{\partial t} = \frac{\alpha_{cr}}{r^2}\frac{\partial}{\partial r}\left(r^2\frac{\partial T_{cr}}{\partial r}\right), \quad R_i(t) \leqslant r \leqslant R_p \tag{7}$$

with R_d and R_i the droplet and crust-wet core interface radius, ρ_w the density of the liquid, h_{fg} the specific heat of evaporation, $c_{p,w}$ the specific heat of the liquid, m_d the mass of the droplet, T_d,T_{wc}, and T_{cr}, respectively, the temperatures of the droplet, the wet core, and the crust region, ρ_{wc} the density of the wet core, $c_{p,wc}$ the specific heat of the wet core, k_{wc} the thermal conductivity of the wet core, and α_{cr} the thermal diffusivity of the crust. The calculation of the parameters is described by Mezhericher et al. [1,20].

1.3. Objectives

This work reports on (1) the development and calibration of a mechanistic model of the drying process of a continuously produced pharmaceutical granule in a six-segmented fluidised bed drying system and (2) the validation of the developed model using independent experiments. The development of this model should be considered as an attempt to build up process knowledge in the frame of a PAT project, which then later on can be used for the definition of a design space and for the development of suitable control strategies to optimally guarantee the end product quality of the drying process that is studied. The development of a mechanistic model is innovative for pharmaceutical applications, as most studies are based on black box models, that is, empirical models containing parameters with no physical meaning. However, recently more and more mechanistic models become available; examples are work on blending [21], granulation [9], film coating [21], etc.

This work is based on the model described by Mezhericker et al. [1]. The added value of this work is the sensitivity analysis, the calibration, the introduction of a submodel to describe the gas temperature dependence of β and the model validation.

2. Materials and methods

2.1. Experimental data

As data collection set-up, the ConsiGma™ continuous from-powder-to-tablet production line from GEA Pharma Systems (Collette™,

Wommelgem, Belgium) was used. The continuous line consists of three parts: a continuous twin-screw granulator (high shear), followed by a six-segmented fluidised bed dryer system and a discharge system.

The formulation of the dry premix consisted of theophylline anhydrate (Farma-Quimica sur SL, Malaga, Spain) (30%, w/w), lactose monohydrate 200 M (DMV fonterra) (67.5%, w/w), and polyvinylpyrrolidone (PVP) (Kollidon 30, BASF, Burgbernheim, Germany) (2.5%, w/w). This premix was granulated with a 0.5% (w/v) sodium lauryl sulfate (SLS) solution (Fagron, Waregem, Belgium) in distilled water at a barrel temperature of 25 °C. SLS was added to improve the wettability of the dry premix. The screw speed was held constant at 950 rpm, the powder mass flow at 10 kg/h, and the liquid mass flow at 18 g/min. The ConsiGma™ standard screw configuration was used. Wet granules were collected in closed vessels.

The fluidised bed dryer (Fig. 1) works in a continuous way and is built up in six segments. The continuous flow of granules, coming from the high shear granulator, fills one segment at a time. After drying for a pre-installed time instant, the segment is emptied and filled again.

Experimental drying data were collected in order to perform a calibration of β followed by a validation of the drying model. To achieve this, continuously produced granules were dried at different drying air temperatures: 35 °C, 40 °C, 50 °C, 60 °C, and 70 °C. The gas flow rate was kept constant at 200 m^3/h. In each drying experiment, a limited amount of equally sized granules were used in order to measure the behaviour of one single granule. This was achieved by using a sieve fraction of the granulated wet granules (1000–1400 μm). During each drying experiment, samples were collected at several drying time instants. In order to achieve this sampling in practice, the drying process was stopped, and the granules were captured and stored in closed vessels.

The moisture content was determined with Karl Fischer titration using a V30 volumetric KF titrator (Mettler Toledo, USA). Before the titration of the granules, these granules were stirred and dissolved (methanol (Hydranal, Sigma Aldrich, Germany)) for 5 min.

During the collection of the experimental data, the humidity of the drying agent (air) and the pressure in the dryer were continuously monitored. During one experiment, the humidity and the pressure can be assumed as being constant, but between the different experiments especially the humidity can vary in a broad range. The measured moisture content corresponding to the early time steps is less reliable and more noisy compared to later time steps. The reason for this is twofold. First, it takes some time to introduce the granules in the dryer body. Secondly, after stopping the drying process, there is a certain delay till the granules can be collected. Water at the surface of the granules can evaporate easily during this delay. At later time instants, the water is less available, because surface water is not present anymore.

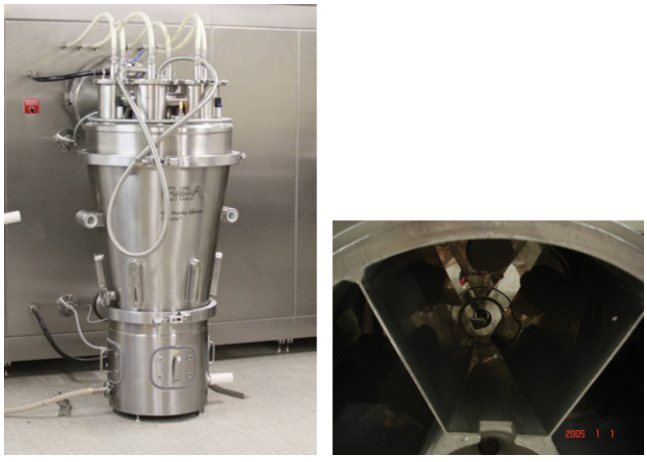

(a) Entire dryer (b) One segment

Fig. 1. ConsiGma™ fluidised bed dryer. (For interpretation of the references to color in this figure legend, the reader is referred to the web version of this article.)

For each experiment, β was determined using the data points of the second drying phase. This was done by minimising the Sum of Squared Errors (SSE) (8) between the experimental data and the model prediction.

$$\mathrm{SSE} = \sum_i (y_i - \hat{y}_i)^2 \tag{8}$$

where y_i is an experimental data point at time t_i and $\hat{y}_i$ is the model prediction at time t_i. With the help of three independent experiments at a gas temperature of 50 °C, 60 °C, and 70 °C, the validation was performed. The experimental set-up for these experiments was similar as for the calibration experiments. The measured moisture content was compared with the predicted result using the calibrated drying model.

2.2. Numerical solution

The first drying period consists of an ODE for the temperature (Eq. (4)), an ODE for the droplet radius (Eq. (3)) and several algebraic equations [20]. The ODE for the temperature is solved using a forward Euler scheme, while the ODE for the droplet radius can easily be solved analytically.

The equations of the second drying period consist of a PDE for the temperature in the dry crust and one for the temperature in the wet core (Eqs. (6) and (7)) with accompanying boundary conditions. An ODE for the decrease in wet core radius (Eq. (5)) is responsible for the moving boundary [1]. The combination of the PDEs and the ODE is solved using the numerical methods described by Illingworth and Golosnoy [22]. The positional variable of the PDEs is first transformed by a Landau transformation. The resulting PDEs are discretised using a fully implicit, conservative finite difference technique, which are solved using a Crank–Nicolson scheme.

2.3. Local sensitivity analysis

A local sensitivity analysis was performed to detect the most sensitive parameters in the model. This information can be used to understand how the input of the model (e.g., a parameter or initial condition) will influence the variation in the output. For this analysis, the central difference scheme was used, as shown in the following equation:

$$\frac{\partial \mathbf{y}(t)}{\partial \theta_{(j)}} = \frac{\mathbf{y}(t, \theta_j + \xi\theta_j) - \mathbf{y}(t, \theta_j - \xi\theta_j)}{2\xi\theta_j} \tag{9}$$

with $y(t, \theta_j)$ the output variable, θ_j the value of the perturbed parameter and ξ the perturbation factor. In this application, the output variable is the moisture content.

The choice of the perturbation factor was based on the sum of the absolute errors [23]. Two sensitivity functions are calculated:

$$\frac{\partial \mathbf{y}(t)}{\partial \theta_{(j,+)}} = \frac{\mathbf{y}(t, \theta_j + \xi\theta_j) - \mathbf{y}(t, \theta_j)}{\xi\theta_j} \tag{10}$$

$$\frac{\partial \mathbf{y}(t)}{\partial \theta_{(j,-)}} = \frac{\mathbf{y}(t, \theta_j) - \mathbf{y}(t, \theta_j - \xi\theta_j)}{\xi\theta_j} \tag{11}$$

The difference between both sensitivity functions should be minimal to ensure that the numerical error and the error introduced by the nonlinearity of the model are as small as possible.

Table 1
Parameters used for the sensitivity analysis.

Parameter	Numerical value
T_g	50 °C
V_g	200 m^3/h
p_g	101,300 Pa
R_p	0.6 mm
Humidity	9%
ϵ	0.05
μ_{gas}	0.00002 kg/m/s
ρ_{gas}	1.2 kg/m^3
k_{gas}	0.0285 W/m/K
cp_{gas}	1009 kg/m^3
ρ_{liquid}	1000 kg/m^3
ρ_{solid}	1525 kg/m^3
$k_{droplet}$	0.07 W/m/K
k_{liquid}	0.63 W/m/K
k_{solid}	0.75 W/m/K
ϵ_{rs}	0.8
β	1.84

This can be used to determine the optimal perturbation factor. Several criteria to quantify this difference exists, and the Sum of Absolute Errors (SAE) and the Sum of Relative Errors (SRE) were used and compared:

$$\mathrm{SAE} = \frac{\sum \left| \frac{\partial y(t)}{\partial \theta_{(j,+)}} - \frac{\partial y(t)}{\partial \theta_{(j,-)}} \right|}{N} \tag{12}$$

$$\mathrm{SRE} = \frac{\sum \left| 1 - \frac{\frac{\partial y(t)}{\partial \theta_{(j,-)}}}{\frac{\partial y(t)}{\partial \theta_{(j,+)}}} \right|}{N} \tag{13}$$

with N the number of datapoints where the sensitivity is evaluated [23].

To evaluate the information about the sensitivity analysis the total relative sensitivity is calculated (Eq. (14)). This enables to compare and rank the sensitivity of the parameters. This ranking can be used to decide on parameters to be used for model calibration (most sensitive parameters) or parameters to be removed from the model (in case the model is not at all sensitive to a parameter).

$$\frac{\partial y(t)}{\partial \theta j)} \frac{\theta j)}{y(t)} \tag{14}$$

The nominal values of the parameters are given in Table 1.

3. Results and discussion

3.1. Experimental data

The collected experimental data are summarised in Table 2. The unit of moisture content is % (kg water/kg total mass).

This data involved the first and the second drying period. Only the data points of the *second drying period* were used for the calibration of β. One data point was eliminated, as it was identified as an outlier.

3.2. Sensitivity analysis

Eq. (2) contains an empirical power coefficient, β. Information about this parameter is not found in literature. However, the influence of this parameter on the evaporation rate is significant. An increase in β causes a decrease in the evaporation rate and, hence, a slower drying process. A sensitivity analysis was performed to determine the contribution of β.

To determine the optimal perturbation factor, the summation of the SAEs and the SREs for all parameters is made. The result is presented in Figs. 2 and 3. According to the SAE criterion, the optimal perturbation factor is 1e−6, whereas according to the SRE criterion, 1e−5 would be choosen. De Pauw et al. concluded that the SRE criterion was useful to assess the quality of sensitivity function calculations [23]. As a consequence, it was decided to use 1e−5 as perturbation factor.

The results of the sensitivity analysis, performed on the parameters, are presented in Fig. 4. The simulation was stopped when the particle was dry (after 270 s). In this time range, the mean of the absolute value of the total relative sensitivity was calculated and presented.

It can be concluded that the gas temperature is the most sensitive parameter, followed by β. It can be noted that the gas temperature determines the drying behaviour for the whole time range of the drying process, whereas the β-parameter only has an influence in the second drying phase (Eqs. (1) and (2)). The major influence of β is important and is in fact rather critical, as there is no information available about this parameter.

3.3. Model calibration

In Fig. 5, the resulting model prediction at each evaluated drying temperature is presented, together with the experimental data.

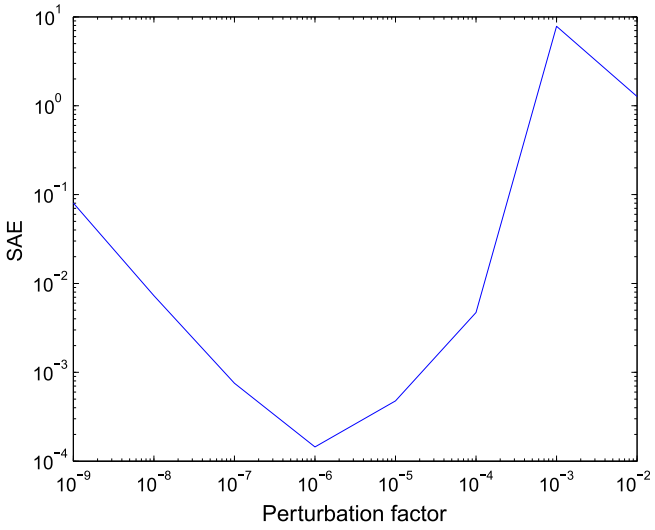

Fig. 2. Criteria values for the SAE. (For interpretation of the references to color in this figure legend, the reader is referred to the web version of this article.)

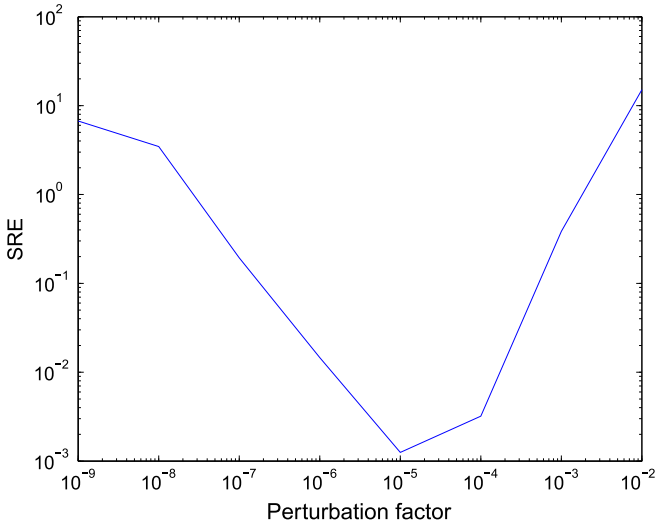

Fig. 3. Criteria values for the SRE. (For interpretation of the references to color in this figure legend, the reader is referred to the web version of this article.)

Table 2
Experimental data. The bold values are used for the model calibration and validation.

35 °C	t (s)	0	1	4	9	13	14	31	84	348	567	
	X (%)	8.46	4.72	3.85	3.58	3.91	3.91	**3.55**	**2.96**	**3.00**	**3.01**	
40 °C	t (s)	0	5	10	20	40	80	200	400	1000		
	X (%)	8.51	3.88	3.40	**3.34**	**2.84**	**2.68**	**2.24**	**2.06**	**1.60**		
45 °C	t (s)	0	2	8	20	50	200	360	720			
	X (%)	8.17	3.33	3.44	**2.96**	**2.50**	**1.73**	**1.84**	**1.21**			
50 °C	t (s)	0	1	5	10	15	40	80	200	720		
	X (%)	8.12	3.86	3.56	**3.04**	**2.33**	**2.37**	**1.75**	**1.35**	**0.22**		
55 °C	t (s)	0	1	2	5	10	15	40	80	200	300	420
	X (%)	8.19	3.57	2.46	2.94	2.84	**2.69**	**1.90**	**1.28**	**1.36**	**0.72**	**0.14**
60 °C	t (s)	0	1	2	5	7	10	15	20	40	80	200
		240	360									
	X (%)	7.75	2.94	2.69	1.77	1.92	**2.16**	0.67	**1.89**	**1.03**	**0.56**	**0.40**
		0.12	**0.05**									
65 °C	t (s)	0	1	5	7	10	15	20	40	80	100	
	X (%)	7.98	2.46	3.77	**1.92**	**2.05**	**1.72**	**1.80**	**0.62**	**0.05**	**0.04**	
70 °C	t (s)	0	1	5	7	10	15	20	40	80		
	X (%)	8.12	4.20	3.66	**2.98**	**2.01**	**1.62**	**1.09**	**0.27**	**0.01**		

The experimental data at 60 °C contained an outlier, and this data point was therefore eliminated prior to performing the parameter estimation.

The goodness-of-fit was determined by calculation of the Theil's Inequality Coefficient (TIC) [24] and the Root Mean Squared Error (RMSE). The TIC and the RMSE are respectively given by:

$$\mathrm{TIC} = \frac{\sqrt{\sum_i (y_i - y_{m,i})^2}}{\sqrt{\sum_i y_i^2}\sqrt{\sum_i y_{m,i}^2}} \tag{15}$$

$$\mathrm{RMSE} = \sqrt{\sum_i (y_i - y_{m,i})^2 / n} \tag{16}$$

where y_i is an experimental data point, $y_{m,i}$ is the model prediction, and n is the number of data points. A TIC value lower than 0.3 indicates a good agreement between the experimental data and the model predictions [25].

The calculated values (Table 3) show that the values of the RMSE and the TIC are in the same range for the five experiments. Both criteria resulted in a similar conclusion with regard to the goodness-of-fit; the model prediction experiment at 70 °C was the best according to the RMSE and TIC, while the worst model prediction was either the experiment at 50 °C (RMSE), or at 60 °C (TIC).

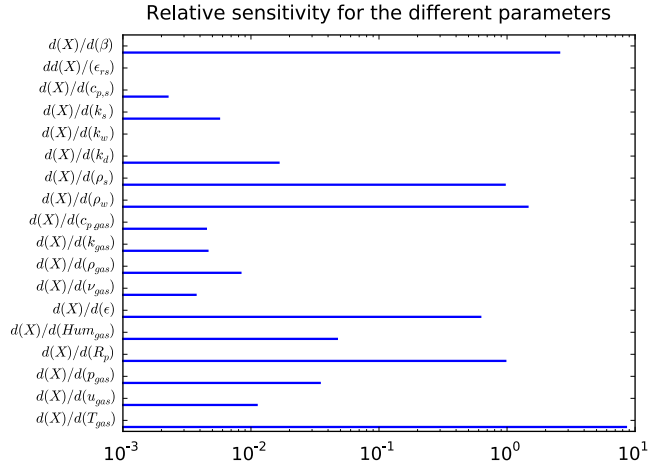

Fig. 4. Results of the sensitivity analysis. (For interpretation of the references to color in this figure legend, the reader is referred to the web version of this article.)

Furthermore, it can be observed that optimal β values exhibited a decreasing trend with increasing gas temperature. This means that the model with a fixed beta value cannot be used to predict drying behaviour at different gas temperatures.

In Fig. 6, the calibrated β-values along with their 95% confidence interval (Eq. (17)) are shown. The calculation of the covariance for the confidence interval is based on the Fisher Information Matrix (FIM). The inverse of the FIM is the lower limit of the parameter estimation error covariance matrix [26], which means that the real confidence interval will be a bit larger.

$$\mathrm{CI} = \beta \pm t_{N-p}^{\alpha} \times \sqrt{C_{ii}} \tag{17}$$

Here, $\sqrt{C_{ii}}$ is the covariance and t_{N-p}^{α} the t-value of the student's t distribution with $N - p$ degrees of freedom and α the significance level. N is the total number of data points, while p is the number of estimated parameters.

It was observed that the confidence interval for the experiment at 35 °C was larger than for the other experiments. As mentioned in Section 2.1, the collected experimental data contain some unreliabilities, which can form an explanation for the difference in size of the confidence interval. It was therefore decided to investigate the relation between β and the gas temperature with and without considering this experiment in order to eliminate the more noisy data.

3.4. Relation between β and the gas temperature

Fig. 6 clearly shows that there is a relation between β and the gas temperature, which seems to be exponential in nature. Therefore, an exponential function was fitted to the data, first for all five calibration experiments (Case A), and then also for the remaining data after excluding the experiment at 35 °C (Case B). The resulting equation for case A is

$$\beta = 4912.4 * e^{-0.024282 * T_{gas}} \tag{18}$$

with T_{gas} the gas temperature in Kelvin.

For case B:

$$\beta = 1117.4 * e^{-0.019854 * T_{gas}} \tag{19}$$

Both fits are shown in Fig. 6. The inclusion of the experiment at 35 °C clearly has a significant impact. The goodness-of-fit of the submodels is in fact a second optimisation problem, where the goal

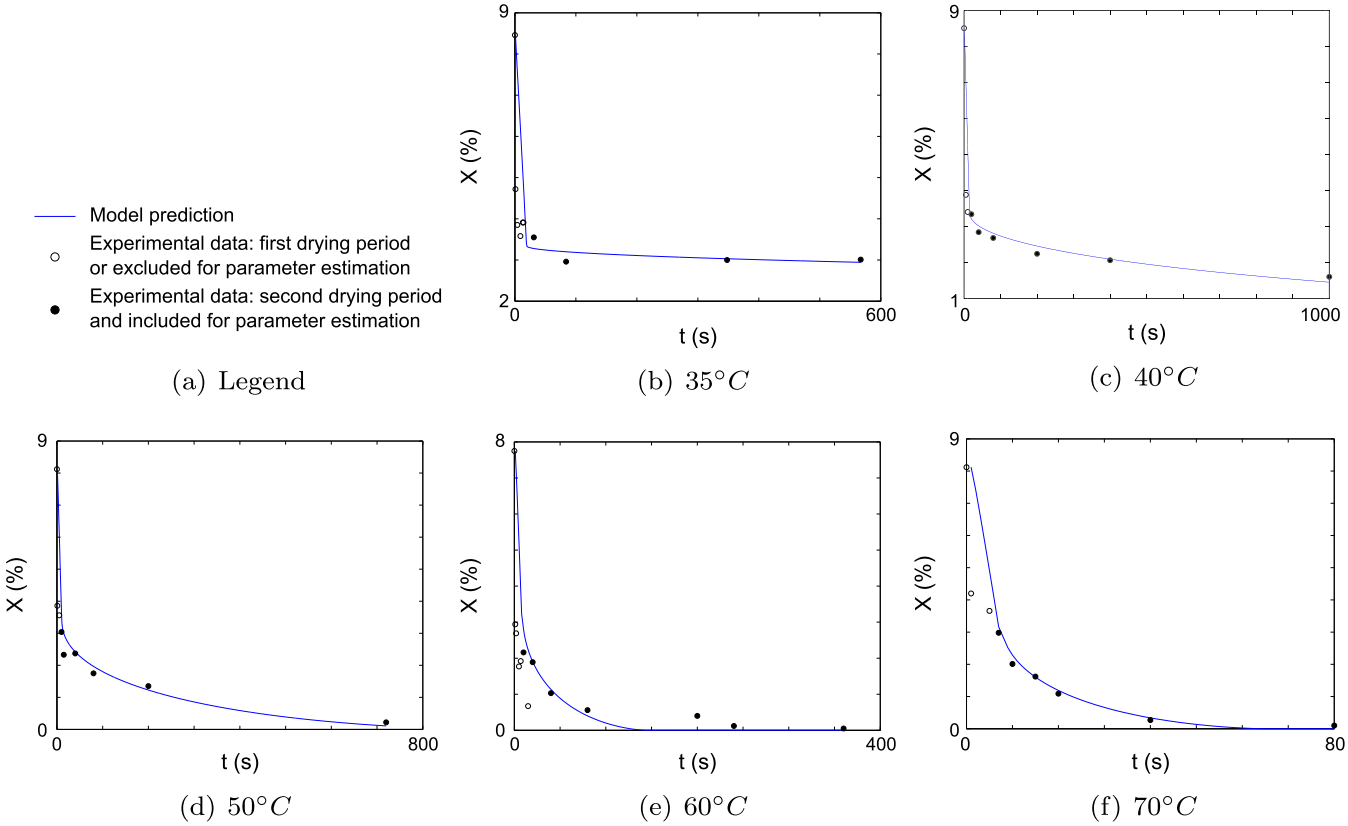

Fig. 5. Calibration of β at different gas temperatures. (For interpretation of the references to color in this figure legend, the reader is referred to the web version of this article.)

Table 3
TIC and RMSE for the calibration experiments.

Experiment	35 °C	40 °C	50 °C	60 °C	70 °C
β	3.088	2.275	1.840	1.389	1.289
RMSE	0.1852	0.1455	0.2998	0.2543	0.09552
TIC	0.02961	0.02864	0.06943	0.1024	0.02882

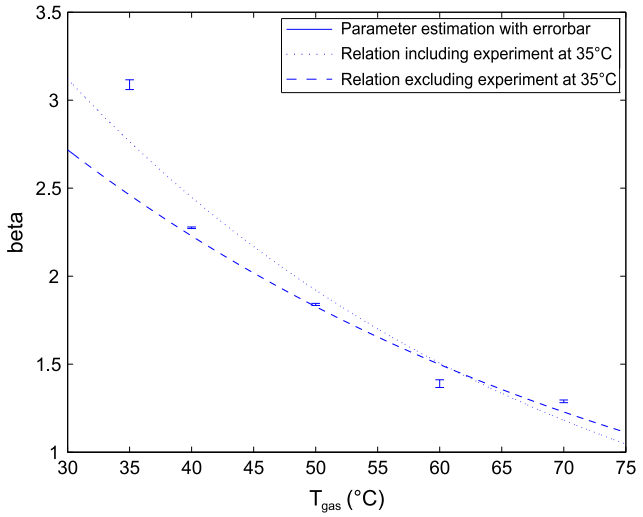

Fig. 6. β–T_{gas} relation: experimental data and model fits for cases A and B. (For interpretation of the references to color in this figure legend, the reader is referred to the web version of this article.)

Table 4
Criteria for the goodness-of-fit of the submodel. The bold values indicates the model with the best performance.

	Case A	Case B
R^2	0.9229	**0.9918**
RMSE	1.8250e−001	**6.6710e−002**
TIC	4.4172e−002	**1.9174e−002**
p-Value	0.9028	**0.9936**

is to find the optimal parameters of the submodel. The goodness-of-fit was determined using R^2, RMSE, TIC, and the p-value of a paired t-test. The performance of the submodel was better when eliminating the experiment at 35 °C for all calculated criteria (Table 4). It should be noted that this might have an impact on model predictions at this temperature as this would be an extrapolation of that model which should be avoided or only be done with the necessary caution.

3.5. Validation

Eqs. (18) and (19) were implemented in Eq. (2), which changed the model structure. The resulting model was used for the validation.

The result of the validation is presented in Fig. 7. At 45 °C and 55 °C, the calculated moisture content for case A was higher compared to case B. The opposite is valid for the validation experiment at 65 °C. In the two validation experiments at the lowest gas temperature, the difference between both model predictions was the largest. At 65 °C, there was almost no difference anymore between both model predictions.

In Table 5, the calculated criteria to determine the goodness-of-fit of the validation are presented. Based on these results it

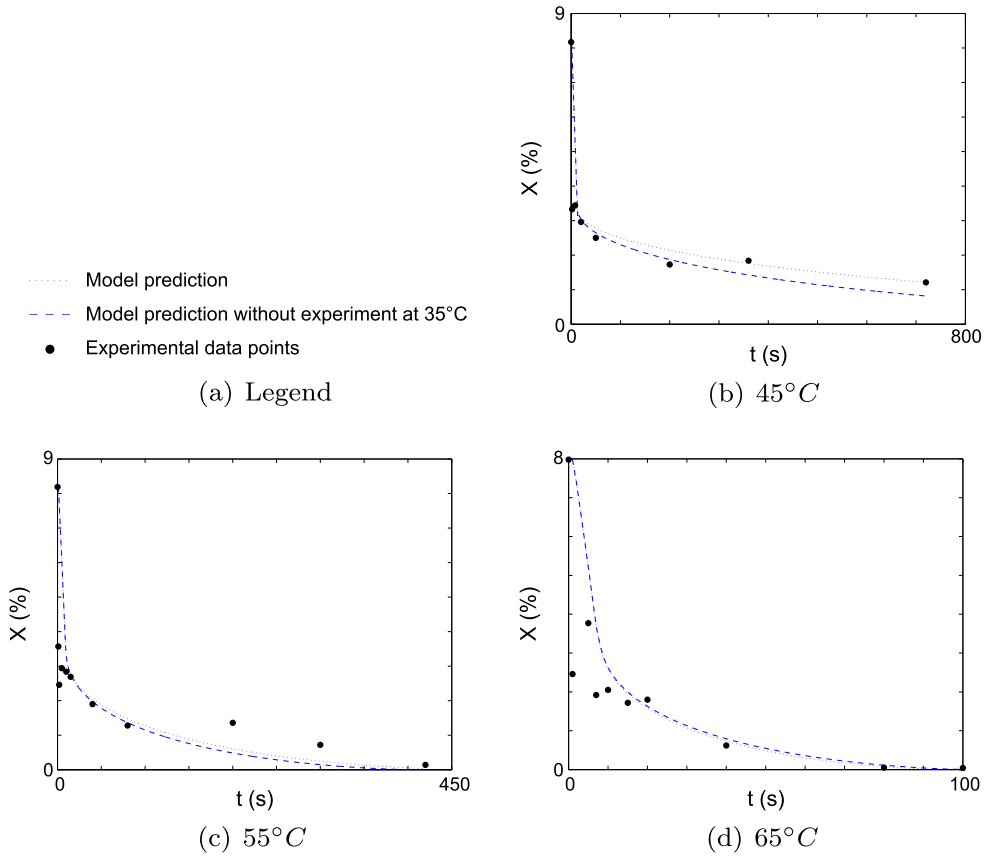

Fig. 7. Validation results. (For interpretation of the references to color in this figure legend, the reader is referred to the web version of this article.)

Table 5
TIC and RMSE for the validation experiments. The bold values indicates the model with the best performance.

	Case A	Case B
Validation experiment 1: 45 °C		
RMSE	**0.1812**	0.2155
TIC	**0.0517**	0.0642
Validation experiment 2: 55 °C		
RMSE	**0.2806**	0.3210
TIC	**0.1219**	0.1426
Validation experiment 3: 65 °C		
RMSE	**0.4330**	0.4370
TIC	**0.1604**	0.1608

can be seen that the performance of the submodel, including the experiment at 35 °C, was better than the performance obtained when excluding this experiment. The value of the RMSE and the TIC are almost equal for the experiment at 65 °C, which could also be seen in Fig. 7. This is in contradiction with the results of Table 4, as it was expected that the submodel excluding the experiment at 35 °C would describe the gas temperature dependency better. As the elimination of the experiment at 35 °C means a loss of information, and in considering also that pharmaceutical applications drying at 35 °C is sometimes necessary in pharmaceutical applications in cases with temperature sensitive drugs, it was decided to include this experiment in the analysis. Hence, the proposed gas temperature dependent drying model is Eq. (18).

Table 6
Summary of the drying model.

Assumptions	Possible input variables	Critical end characteristics
Spherical granules	Gas temperature	Moisture content of the granule X (kg water/kg total mass)
Spherical wet core	Gas flow rate	Temperature distribution in the granule
Constant particle radius	Gas humidity	Mass of the granule (kg)
	Pressure in the dryer	Density of the granule (kg granule/m^3 granule)
	Granule radius	
	Porosity of the granule (Volume gas of a dried granule per total volume of the granule)	
	Initial moisture content of the particle	
	Density of the solid phase	
	Thermal conductivity of the solid phase	
	Specific heat of the solid	
	Dynamic viscosity of the gas	
	Density of the gas	
	Thermal conductivity of the gas	
	Specific heat of the gas	

4. General conclusion

The drying behaviour of pharmaceutical granules can be modelled with the drying model as presented by [1]. The drying behaviour elapses in two phases, which gives rise to two submodels in the mechanistic drying model. In the first drying phase, the surface water evaporates, while in the second drying phase, the water inside the granule evaporates. The submodel of the second drying phase consists of an empirical power coefficient,β; however, no information about this parameter was found in literature. Based on a sensitivity analysis, it can be concluded that β has a significant influence on the moisture content of the granule.

In this work, the aim was to calibrate the β-parameter by means of drying experiments with a continuous fluidised bed dryer. Based on five experiments, an exponential dependence of β on the gas temperature was found.

The resulting model was validated using experimental data of independent experiments at different gas temperatures. The resulting validated drying model is able to predict the evolution of the moisture content for one single granule (Table 6).

The validated drying model can now be used in further research. The model can be extended towards a certain amount of granules, meaning the implementation in a Population Balance Equation (PBE), to investigate the distribution in moisture content of the granule. This distribution is important for the subsequent tabletting step.

Acknowledgment

Financial support for this research from the Fund for Scientific Research Flanders (FWO Vlaanderen – aspirantmandaat Séverine Thérèse F.C. Mortier) is gratefully acknowledged.

References

[1] M. Mezhericher, A. Levy, I. Borde, Theoretical drying model of single droplets containing insoluble or dissolved solids, Dry. Technol. 25 (6) (2007) 1025–1032, doi:10.1080/07373930701394902. <http://www.informaworld.com/openurl?genre=article&doi=10.1080/07373930701394902&magic=crossref||D404A21C5BB053405B1A640AFFD44 AE3>.

[2] H. Leuenberger, New trends in the production of pharmaceutical granules: batch versus continuous processing, Eur. J. Pharm. Biopharm. 52 (3) (2001) 289–296. <http://www.ncbi.nlm.nih.gov/pubmed/11677071>.

[3] K. Plumb, Continuous processing in the pharmaceutical industry changing the mind set, Chem. Eng. Res. Des. 83 (6) (2005) 730–738, doi:10.1205/cherd.04359. <http://linkinghub.elsevier.com/retrieve/pii/S0263876205727 556>.

[4] S. Mortier, T. De Beer, K. Gernaey, J. Remon, C. Vervaet, I. Nopens, Mechanistic modelling of fluidized bed drying processes of wet porous granules: a review, Eur. J. Pharm. Biopharm. 79 (2011) 205–225, doi:10.1016/j.ejpb.2011.05.013. <http://www.ncbi.nlm.nih.gov/pubmed/21664970<.

[5] S. Schaber, D. Gerogiorgis, R. Ramachandran, J. Evans, P. Barton, B. Trout, Economic analysis of integrated continuous and batch pharmaceutical manufacturing: a case study, Ind. Eng. Chem. Res. 50 (17) (2011) 10083–10092.

[6] D. Roberge, L. Ducry, N. Bieler, P. Cretton, B. Zimmermann, Microreactor technology: a revolution for the fine chemical and pharmaceutical industries?, Chem Eng. Technol. 28 (3) (2005) 318–323, doi:10.1002/ceat.200407128. <http://doi.wiley.com/10.1002/ceat.200407128>.

[7] G. Sin, P. Odman, N. Petersen, A. Lantz, K. Gernaey, Matrix notation for efficient development of first-principles models within PAT applications: integrated modeling of antibiotic production with streptomyces coelicolor, Biotechnol. Bioeng. 101 (1) (2008) 153–171, doi:10.1002/bit.2186. <http://www.ncbi.nlm.nih.gov/pubmed/18454503>.

[8] K. Gernaey, R. Gani, A model-based systems approach to pharmaceutical product-process design and analysis, Chem. Eng. Sci. 65 (21) (2010) 5757–5769, doi:10.1016/j.ces.2010.05.00. <http://dx.doi.org/10.1016/j.ces.2010.05.003>.

[9] F. Boukouvala, A. Dubey, A. Vanarase, R. Ramachandran, F. Muzzio, M. Ierapetritou, Computational approaches for studying the granular dynamics of continuous blending processes. 2 – Population balance and data-based methods, Macromol. Mater. Eng. 296 doi:10.1002/mame.201100054. <http://doi.wiley.com/10.1002/mame.201100054>.

[10] F. Muzzio, T. Shinbrot, B. Glasser, Powder technology in the pharmaceutical industry: the need to catch up fast, Powder Technol. 124 (2002) 1–7.

[11] A. Hegedus, K. Pintye-Hódi, Comparison of the effects of different drying techniques on properties of granules and tablets made on a production scale, Int. J. Pharm. 330 (1-2) (2007) 99–104, doi:10.1016/j.ijpharm.2006.09.00. <http://www.ncbi.nlm.nih.gov/pubmed/17049769>.

[12] P. Perré, I. Turner, The use of macroscopic equations to simulate heat and mass transfer in porous media, in: I. Turner, A. Mujumdar (Eds.), Mathematical Modeling and Numerical Techniques, New York, 1996, pp. 83–156.

[13] P. Perre, I. Turner, A 3-D version of TransPore: a comprehensive heat and mass transfer computational model for simulating the drying of porous media, Int. J. Heat Mass Transfer 42 (24) (1999) 4501–4521, doi:10.1016/S0017-931(99)00098-8. <http://linkinghub.elsevier.com/retrieve/pii/S0017931099000988>.

[14] F. Couture, P. Fabrie, J.R. Puiggali, An alternative choice for the drying variables leading to a mathematically and physically well described problem, Dry. Technol. 13 (3) (1995) 519–550, doi:10.1080/07373939508916973. <http://www.informaworld.com/10.1080/07373939508916973>.

[15] N. Boukadida, S. Nasrallah, Two dimensional heat and mass transfer during convective drying of porous media, Dry. Technol. 13 (3) (1995) 661–694, doi:10.1080/07373939508916979. <http://www.informaworld.com/10.1080/07373939508916979>.

[16] M. Prat, Recent advances in pore-scale models for drying of porous media, Chem. Eng. J. 86 (1-2) (2002) 153–164, doi:10.1016/S1385-8947(01)00283-2. <http://linkinghub.elsevier.com/retrieve/pii/S1385894701002832>.

[17] F. Plourde, M. Prat, Pore network simulations of drying of capillary porous media. Influence of thermal gradients, Int. J. Heat Mass Transfer 46 (7) (2003) 1293–1307, doi:10.1016/S0017-9310(02)00391-. <http://linkinghub.elsevier.com/retrieve/pii/S0017931002003915>.

[18] H. Huinink, L. Pel, M. Michels, M. Prat, Drying processes in the presence of temperature gradients – pore-scale modelling, Eur. Phys. J. E 9 (5) (2002) 487–498, doi:10.1140/epje/i2002-10106-. <http://www.ncbi.nlm.nih.gov/pubmed/15011097>.

[19] A. Yiotis, A. Stubos, A. Boudouvis, Y. Yortsos, A 2-D pore-network model of the drying of single-component liquids in porous media, Adv. Water Resour. 24 (3–4) (2001) 439–460, doi:10.1016/S0309-1708(00)00066. <http://linkinghub.elsevier.com/retrieve/pii/S030917080000066X>.

[20] M. Mezhericher, A. Levy, I. Borde, Modelling of particle breakage during drying, Chem. Eng. Process. 47 (8) (2008) 1404–1411, doi:10.1016/j.cep.2007.06.01. <http://linkinghub.elsevier.com/retrieve/pii/S0255270107002188>.

[21] W. Ketterhagen, M. Am Ende, B. Hancock, Process modeling in the pharmaceutical industry using the discrete element method, J. Math. Psychol. 98 (2) (2009) 442–470, doi:10.1002/jps.

[22] T. Illingworth, I. Golosnoy, Numerical solutions of diffusion-controlled moving boundary problems which conserve solute, J. Comput. Phys. 209 (1) (2005) 207–225, doi:10.1016/j.jcp.2005.02.03. <http://linkinghub.elsevier.com/retrieve/pii/S0021999105000859>.

[23] D. De Pauw, P. Vanrolleghem, Practical aspects of sensitivity function approximation for dynamic models, Math. Comput. Model. Dyn. Syst. 12 (5) (2006) 395–414, doi:10.1080/1387395060072330. <http://www.tandfonline.com/doi/abs/10.1080/13873950600723301>.

[24] H. Theil, Economic Forecasts and Policy, North-Holland Publishing Company, Amsterdam, 1961.

[25] W. Audenaert, M. Callewaert, I. Nopens, J. Cromphout, R. Vanhoucke, A. Dumoulin, P. Dejans, S. Van Hulle, Full-scale modelling of an ozone reactor for drinking water treatment, Chem. Eng. J. 157 (2–3) (2010) 551–557, doi:10.1016/j.cej.2009.12.05. <http://dx.doi.org/10.1016/j.cej.2009.12.051>.

[26] D. Dochain, P. Vanrolleghem, Dynamical Modelling and Estimation in Wastewater Treatment Processes, IWA Publishing, 2001.